Statistical and Spectral Modelling of Medium Grazing Angle Coherent Radar Data

Michael McDonald
Defence Research & Development Canada (DRDC)
Ottawa, Canada
Mike.Mcdonald@drdc-rddc.gc.ca

Delphine Cerutti-Maori
Fraunhofer FHR
Wachtberg, Germany
Delphine.Cerutti-Maori@fhr.fraunhofer.de

***Abstract*—The statistical and spectral characteristics of medium grazing angle radar sea clutter data are examined. A clutter model comprised of two independent K-distributed spectral components is found to provide a good fit to observed radar clutter echo characteristics when Doppler broadening due to platform motion is considered. The two-component model is shown to be incompatible with the SIRP model which is frequently utilised for coherent detector development.**

***Index Terms*—Radar, GMTI, Maritime surveillance, Sea clutter analysis, STAP.**

I. Introduction

Airborne wide area, maritime surveillance has traditionally been accomplished using nonconherent high bandwidth radar systems operating from low altitude aircraft at low grazing angles. As such the characterisation of maritime radar clutter returns has predominantly focused on noncoherent statistics corresponding to low grazing angle geometries. The migration of maritime surveillance activities from traditional low flying fixed wing platforms to high altitude platforms, such as UAVs and aerostats, will require that the statistical and spectral characteristics of the high grazing angle (HGA) and medium grazing angle (MGA) regimes be carefully studied and modelled to provide guidance in the specification and design of maritime surveillance radars for next generation platforms. In this paper we characterise a MGA real coherent data set collected using the Fraunhofer FHR phased-array multi-functional imaging radar (PAMIR) to determine the spectral and statistical characteristics as a function of Doppler frequency. A two-component model is fitted to the data to provide a phenomenological explanation of the underlying clutter mechanisms which give rise to the observed characteristics. The fitted model provides insights into the limitations of currently utilised coherent clutter models and the associated detector development.

II. Data Set

The data underlying this analysis was acquired using the Fraunhofer FHR PAMIR system operating in a scan-MTI mode in a sidelooking configuration [1], [2]. During the collection trial the radar platform flew at an altitude of 2500 m (8200 feet) with a velocity of 100 m/s. The antenna grazing angle was approximately 20°. Two data collection passes (see Figure 1) were undertaken with look directions corresponding to approximately downwind (pass 1) and upwind (pass 2) geometries, i.e., wind is blowing away from or towards the radar antenna pointing direction, respectively. The trial took place in the North Sea between Helgoland and Wilhelmshaven in Germany in December, 2009. Key operating parameters and collection geometry details are provided in Table I. Sea conditions were moderate with a reported swell height of 0.9-1.5 m and a wind sea wave height of 0.4-0.5 m.

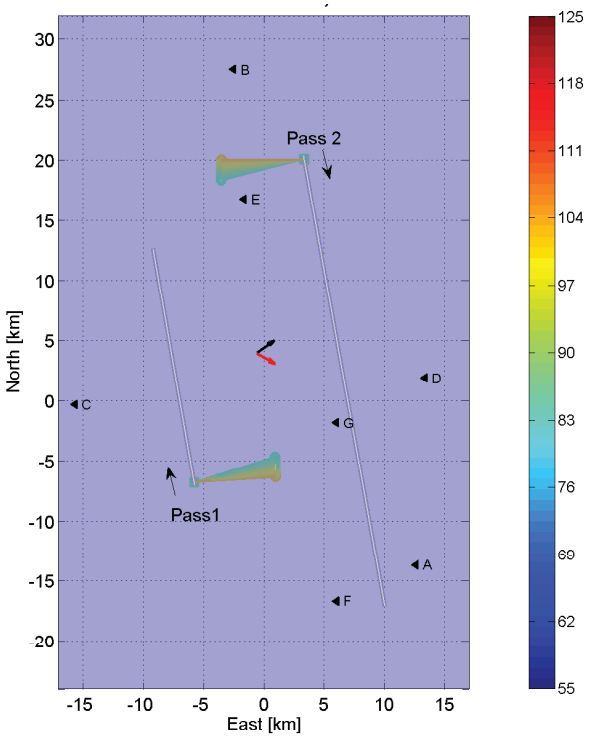

Fig. 1. Flight geometries in the East-North-Up coordinate system. Wind direction and swell direction are indicated by the black and the red arrows, respectively. The color codes the steering direction [°] of the antenna.

III. Measured Spectra and Statistics of Sea Clutter Returns

Figure 2 presents mean sea clutter spectra derived from the PAMIR data. Several characteristics are immediately apparent:

978-1-4673-9655-4/15/$31.00

TABLE I
OPERATING PARAMETERS AND COLLECTION GEOMETRY FOR PAMIR DATA SET

Mean range from aircraft to target	7.3 km
Viewing geometry	Sidelooking looking wrt aircraft motion
Aircraft altitude	2500 m (8200')
Grazing angle	20^o
Platform velocity	100 m/s
Range resolution	7.5 m
Transmit frequency	9.09 & 9.50 GHz
Antenna azimuth	80 cm
Number of channels	3
Antenna phase centre separation	26.6 cm
Antenna TX & RX polarisation	V-V
Coherent processing interval (CPI)	42.6 ms
Effective pulse repetition frequency (PRF)	3 kHz
Centre point of the data take	(53.98 N, 7.91 E)

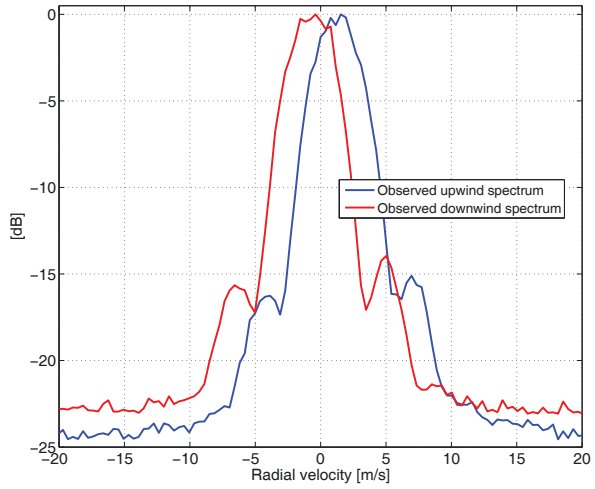

Fig. 2. Upwind and downwind mean spectral power versus Doppler velocity. Peaks of spectra have been normalised to be 0 dB.

1) Upwind clutter response is stronger than downwind clutter response.
2) Spectra peaks are not aligned with 0 Hz. Downwind and upwind display opposite frequency offsets.
3) The spectral shape is highly reminiscent of the antenna beam pattern.

All of these features are anticipated from previous low grazing angle studies. It is well known that radar sea clutter returns are typically stronger form the upwind direction in comparison with the downwind direction [3], furthermore clutter spectra are also known to be shifted in Doppler due to the inherent motion of the scattering mechanisms [4]–[6]. This latter point will be elaborated on in the following discussion.

The last observation with regards to the resemblance of the spectral shapes to the antenna beam pattern arises due to the well known Doppler beam spreading effect which occurs when real data is collected from a moving platform [7]. This issue has been discussed extensively in the literature on space time adaptive processing (STAP), see for instance [8], but is very briefly discussed below to provide context with regards to radar sea clutter measurements.

The Doppler broadening effect is illustrated in Figure 3. The top panel presents the two-dimensional angle versus Doppler representation of the reflected signal from the sea surface for a radar with similar characteristics to the the PAMIR system. A bimodal inherent clutter spectrum, i.e., with local peaks at two distinct Doppler frequencies, has been assumed for reasons which will be clarified later in the paper. The angular slant of the 2D pattern arises due to the fact that clutter returns arriving from different azimuth patches have different Doppler shifts proportional to the radial component of velocity that exists between the moving platform and azimuth location on ground. The inherent spectrum, which is defined at the spectrum that would be observed from a stationary platform, is presented in the bottom panel of Figure 3 and corresponds to a slice through the pattern at a constant azimuth angle. In contrast to this relatively narrow inherent spectrum, the blue curve in the middle panel of Figure 3 corresponds to the projection of the 2-D response onto the Doppler axis and represents the highest resolution spectral response that could be measured by a single channel system from a moving platform. It can thus be seen that the measured mean spectral response of Figure 2 represents a convolution of the antenna pattern with the inherent spectrum. The broader the Doppler spread of the antenna pattern in comparison with the inherent spectrum the more heavily its shape is reflected in the final Doppler broadened spectra. It is interesting to compare the response from a bimodal versus unimodal (the red curve in the middle panel of Figure 3) inherent spectra. The red curve in the bottom panel of Figure 3 corresponds to the Doppler broadened response of the unimodal spectra. Although the bimodal response is slightly broader and shifted with respect to the unimodal it is not readily apparent from visual inspection that these differences arise due to the bimodalism. Indeed it is the authors' experience that similar observed bimodal responses are frequently assumed to arise from a broad unimodal inherent spectrum. Nevertheless, as will be discussed below, the presence of a bimodal spectra can have implication with regards to statistical behaviour of clutter response versus Doppler frequency.

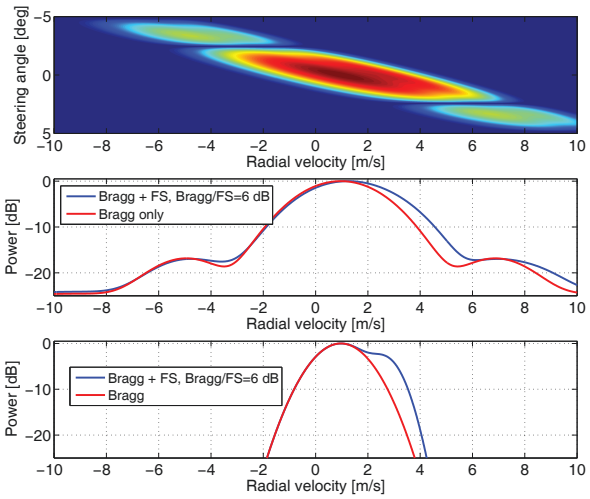

Fig. 3. Doppler versus angle spectral characteristics. Top: Two dimensional angle versus Doppler spectral pattern due to reflection from sea clutter. Middle: Projection of two dimensional angle versus Doppler spectral pattern onto Doppler axis. Blue curve corresponds to Doppler broadened bimodal spectrum. Red curve corresponds to Doppler broadened unimodal spectrum. Bottom: Inherent spectra models. Blue curve corresponds to bimodal inherent spectrum. Red curves corresponds to unimodal inherent spectrum.

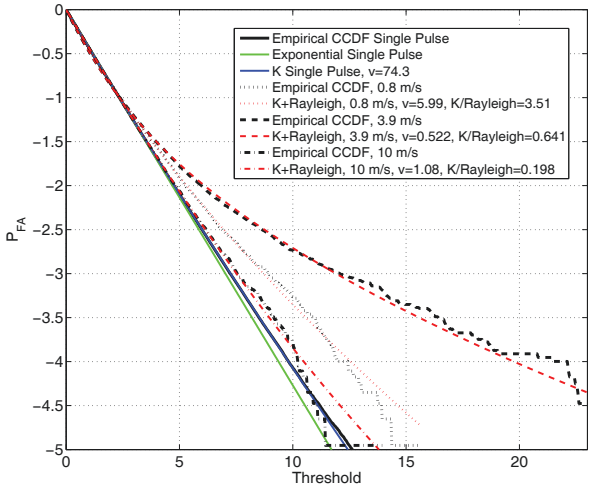

Fig. 4. CCDF curves for PAMIR data for single pulse and selected frequency bins after application of FFT. Upwind viewing geometry.

To better understand the implications of a bimodal spectrum we note that the bimodal sea clutter spectral responses has frequently been associated with the presence of two independent clutter generation mechanisms, each producing a scattered signal response with a different centre Doppler frequencies and spectral width [4]–[6]. The lower frequency response is typically associated with a Bragg scattering mechanism resulting from surface capillary waves while the higher Doppler frequency, or fast scatter (FS) response, has been associated with nonlinear effects due to surface gravity waves. A variety of mechanisms for the generation of FS responses have been proposed but for the purposes of this paper we will not attempt to distinguish between mechanisms and will group all sources under the term FS effects. As alluded to above, the presence of two scattering mechanisms can have a significant impact on underlying statistical behaviour of the clutter, which in turn has implications with respect to detector design and CFAR performance.

To observe the statistical effects we have plotted a series of probability of false alarm (PFA) versus threshold curves (i.e. cumulative complementary distribution functions (CCDF)) in Figure 4 for the upwind direction. The solid black curve in Figure 4 corresponds to the empirical CCDF observed for the noncoherently detected returns and the corresponding solid green and blue curves present exponential and K distributions fitted via moments based methods [3]. The noncoherent fits indicate that the statistics are well approximated by Rayleigh statistics.

We next examine the statistical behaviour versus Doppler frequency by taking the fast Fourier transform (FFT) of a 64 pulse coherent processing interval (CPI) and examine the resulting statistics within each resulting Doppler frequency bin. For conciseness and clarity the results are plotted for only a few selected frequencies in Figure 4. It is readily apparent that statistical behaviour can vary significantly between Doppler bins. For individual Doppler bin results, both the exponential and K distribution fits (not shown) where found to produce poor fits to the empirical CCDFs. To achieve reasonable fits a Rayleigh plus K (RpK) distribution was instead assumed [3]. Comparing the results of Figures 2 and 4 we note that there is a rough correlation between clutter signal strength and increased spikiness, i.e. long CCDF high amplitude tails, although the correspondence is not exact as will be discussed in section IV below. Table III summarises the fitted values for the RpK. The above observations have serious implications for detector design and performance. Sea clutter returns which would be considered to have benign statistical properties, i.e. Rayleigh, under noncoherent detection become much more spiky and variable under coherent detection.

It is tempting to try to associate the fitted Rayleigh and K distribution components with the Bragg and FS clutter mechanisms described above. Ward and Tough [9] postulate a similar association for noncoherent clutter but the consistency of this assignment for the current data is contradicted by the large variation of fitted K shape parameter between Doppler bins. For instance, if a particular mechanism was indeed the sole generator of the fitted K distributed component then one would expect the fitted shape parameter for this component to remain relatively constant across all Doppler bins since the underlying mechanism is unchanged. This point will be discussed further in section V below. Therefore the observations highlight an important caveat with regards to fitting of data to stochastic models; it is commonly observed that the use of a reasonable distribution which has more degrees of freedom (i.e. more characteristic parameters) will produce a better fit to a data set than a distribution with fewer parameters. Quite simply

TABLE II
FITTING PARAMETERS FOR TWO-COMPONENT MODEL INCLUDING K SHAPE PARAMETER AND K COMPONENT POWER TO BRAGG COMPONENT POWER RATIO (K/B RATIO).

(a) Downwind

Doppler velocity	KpR shape	KpK shape	KpR K/B ratio	KpK K/B ratio
-10 m/s	46	12,4	0.5	1.3
-3.9 m/s	0.5	12,4	0.3	5.7
-0.8 m/s	0.8	12,4	0.3	0.2

(b) Upwind

Doppler velocity	KpR shape	KpK shape	KpR K/B ratio	KpK K/B ratio
10 m/s	40	9, 1	0.2	3.9
3.9 m/s	0.5	9,1	0.6	1.9
0.8 m/s	6	9,1	3.5	0.08

more parameters can be adjusted to achieve a better fit. This does not imply that a distribution with more parameters is in fact more representative of the underlying physical reality and the end result may be that a model which shows a good fit to a particular batch of data will yield poor results when an attempt is made to extrapolate its predictions to other conditions and data sets.

IV. TWO-COMPONENT MODEL FIT TO SPECTRA AND SHAPE PARAMETER

Motivated by the observations of the previous section, we now attempt to develop an underlying physical model which explains the variations of both the observed spectral power and stochastic characteristics with Doppler frequency. To achieve this we propose a two-component clutter model consisting of the aforemention Bragg and FS components plus receiver noise. The 'observable' measurements which need to be fitted are spectrum and effective shape parameter. The effective shape parameter was defined by Watts [10] as a tool for dealing with interference composed of K-distributed sea clutter and Rayleigh noise and is derived from the parameters of the Rayleigh plus K distribution fits discussed above. In this paper we now further assume each component to have a simple Gaussian shaped inherent spectrum which is then broadened due to Doppler spreading due to aircraft motion. The observed spectrum and effective shape parameter are plotted versus frequency in Figure 5 for the upwind direction. During the course of the fitting activity it was found that the assumption of Rayleigh and K distributed clutter components led to quite poor fits and it was necessary to allow both clutter components to take the more general form of K distributions. The resulting model assumes two independent clutter components, each with K-distributed statistics and simple Gaussian shaped inherent spectra as discussed above. This will be referred to as a K plus K model (KpK). Based on these assumptions, the model requires the determination of the following fitting parameters: spectral width and centre frequency of each clutter component spectrum, FS to Bragg power ratio and shape parameter of FS and Bragg components. All these parameters are determined during the fitting process with extra weight given to achieving a good spectral power match across the main clutter lobe i.e. across the region in which CNR is greatest. The fitted results are compared against measured values in Figure 5.

The result of the fitting exercise are summarised in Table III for the upwind and downwind directions while Figure 5

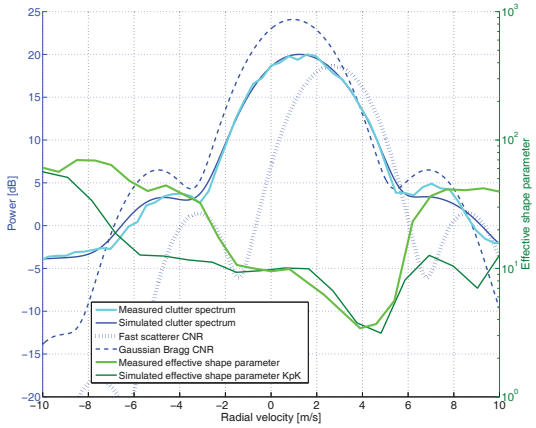

Fig. 5. Comparison of measured effective shape parameter and measured spectrum to fitted spectra and estimated effective shape parameter per KpK models for upwind viewing geometry.

presents plots of the fitted results for the upwind direction. Similar quality fits are achieved for the downwind direction but are not shown for conciseness. Both predicted total spectrum (i.e. sum of component powers), and predicted shape parameter versus frequency are plotted. It can be seen that a very close match is achieved between modelled and observed total spectral power across the main antenna lobe, likewise the effective shape parameter. It is noted that the inclusion of effective shape parameter as an observable strongly constrains the fitted outcome. When this constraint is ignored it was found that relatively good fits to the spectral response can be obtained for a large range of spectral widths, centre frequency and FS to Bragg power ratios. This highlights a difficulty in other reported two-component fits to broadened spectra which rely purely on power spectra [11]. While other ground based measurements utilize polarization ratios to distinguish between different underlying clutter processes [4]–[6], a two-component fit based purely on spectral models can only speculate that two classes of clutter mechanisms are present, for example it could be that only one clutter component with a complex spectral shape is present.

There are few observations of note that can be drawn from the fitted results of Figure 5. The local minimums of endoclutter effective shape parameter do not coincide with

TABLE III
FITTING PARAMETERS FOR TWO-COMPONENT MODEL

	FS velocity	FS width	FS shape	Bragg velocity	Bragg width	Bragg shape KpK fit	FS to Bragg ratio	CNR
Upwind	2.7 m/s	$\pm$0.6 m/s	1.3	1.0 m/s	$\pm$1 m/s	9	-6 dB	13.5 dB
Downwind	-2.0 m/s	$\pm$0.4 m/s	4	-0.3 m/s	$\pm$0.8 m/s	11.5	-4.8 dB	11.5 dB

the peak spectral powers of the clutter components, rather they occur at the points where the ratio of clutter component powers are highest. The success of the model in producing an accurate fit supports the discussion of section III where it is speculated that the independent RpK fits represent a mathematical convenience rather than an accurate representation of the underlying clutter components. The corresponding values from the two-component behaviour are summarised in table III for comparison with the Rayleigh plus K results. The variation of shape parameter with velocity for the RpK fits contrasts with the constancy of the two-component model (where shape parameter is fixed by design). In addition it can be seen that the component power ratios estimated from the independent RpK fits bear little resemblance to the ratios arising from the two-component model.

V. IMPLICATIONS FOR SIRP MODEL

A commonly applied stochastic model for coherent sea clutter processes is the spherically invariant random process (SIRP), which is frequently proposed as a tractable statistical characterisation of the complex envelope of the sea clutter radar echo returns. The SIRP can be viewed as a complex analog to the compound-Gaussian formulations which is commonly applied to non-coherent data. The SIRP can be written as

$$p(\mathbf{z}) = \int_0^\infty \frac{1}{\pi^Q |\tau \mathbf{M}|} e^{-\frac{\mathbf{z}^\dagger \mathbf{M}^{-1} \mathbf{z}}{\tau}} p_{\boldsymbol{\tau}}(\tau) \mathrm{d}\tau, \qquad (1)$$

where $\mathbf{M}$ denotes the normalized covariance matrix and Q is the length of the complex space-time measurement vector $\mathbf{z}$. The variable τ models the power or texture which has a distribution given by $p_{\boldsymbol{\tau}}(\tau)$ [12], [13]. The frequently successful application of compound-Gaussian formulations towards the modelling of noncoherent clutter statistics likely motivates the application of the SIRP to coherent clutter but upon careful consideration of the results presented above it should be apparent that some of the implicit assumptions underlying the SIRP formulation are observed to be violated in real data. Perhaps the most important is the SIRP assumption that the underlying power (in the absence of any added noise) remains constant across the CPI corresponding to a single measurement vector $\mathbf{z}$. This implies that a common power scaling factor affects all spectral components of the underlying clutter equally, i.e., the underlying power spectrum from different realisations of the measurement vector will be identical up to a common scalar in the absence of receiver noise. Clearly this condition contradicts the assumption of two independent clutter components per the model presented above. Other more direct clues indicate that the clutter response is not a SIRP. For instance, in the presence of receiver noise the spikiest Doppler bin would be expected to coincide with the peak of total clutter spectrum for SIRP clutter, this is not observed and is a direct result of the presence and interaction of at least two clutter components. In fact, SIRP processes (in the absence of added receiver noise) would be expected to exhibit identical shape parameters across all Doppler bins. Referring to the fitted clutter components in Figure 5 it is easy to anticipate that this will not be the case for the two-component model as the overall effective shape parameter will vary as a function of the ratio of the component powers versus Doppler frequency.

VI. CONCLUSIONS

It was demonstrated that the spectral and statistical characteristic of real medium grazing angle radar sea clutter data versus Doppler frequency were best explained using a two-component clutter model composed of two independent K-distributed responses with different centre frequencies and different shape parameters. In particular, the observed variation of effective shape parameter in the real data versus frequency is inconsistent with the properties of a SIRP. As such, detector formulations based on an assumption of underlying SIRP processes will likely exhibit degradation of performance and, in particular, departures from CFAR behaviour.

ACKNOWLEDGEMENT

Thanks is extended to all members of the NATO SET 185 Technical Group whose feedback and insights assisted greatly in the development of the results presented in this paper.

REFERENCES

[1] D. Cerutti-Maori, J. Klare, A. R. Brenner, and J. H. G. Ender, "Wide area traffic monitoring with the sar/gmti system pamir," IEEE Transactions on Geoscience and Remote Sensing, vol. 46, no. 10, pp. 3019–3030, October 2008.

[2] M. Mcdonald, D. Cerutti-Maori, and A. Damini, "Characterisation and cancellation of medium grazing angle sea clutter," in Radar Conference (EuRAD), 2010 European, 2010, pp. 172–175.

[3] K. D. Ward, R. J. A. Tough, and S. Watts, "Sea clutter: Scattering, the k distribution and radar performance," Waves in Random and Complex Media, vol. 17, no. 2, pp. 233–234, 2007. [Online]. Available: http://www.tandfonline.com/doi/abs/10.1080/17455030601097927

[4] D. Walker, "Experimentally motivated model for low grazing angle radar doppler spectra of the sea surface," IEE Proc F, Radar Sonar Navig., vol. 147, no. 3, pp. 114–120, 2000.

[5] ——, "Doppler modelling of radar sea clutter," Radar, Sonar and Navigation, IEE Proceedings -, vol. 148, no. 2, pp. 73–80, Apr 2001.

[6] T. Lamont-Smith, K. Ward, and D. Walker, "A comparison of em scattering results and radar sea clutter," in RADAR 2002, Oct. 2002, pp. 439–443.

[7] J. Ward, "Space-time adaptive processing for airborne radar," in Space-Time Adaptive Processing (Ref. No. 1998/241), IEE Colloquium on, 1998, pp. 2/1–2/6.

[8] ——, "Space-time adaptive processing for airborne radar," Lincoln Laboratory, MIT, Technical report 1015, December 1994.

[9] K. D. Ward and R. J. Tough, "Radar detection performance in sea clutter with discrete spikes," in International Radar Conference. IEE, 2002.
[10] S. Watts, "Radar detection prediction in k-distributed sea clutter and thermal noise," Aerospace and Electronic Systems, IEEE Transactions on, vol. AES-23, no. 1, pp. 40–45, 1987.
[11] L. Rosenberg, "Characterization of high grazing angle x-band sea-clutter doppler spectra," Aerospace and Electronic Systems, IEEE Transactions on, vol. 50, no. 1, pp. 406–417, January 2014.
[12] E. Conte and M. Longo, "Characterisation of radar clutter as a spherically invariant random process," Communications, Radar and Signal Processing, IEE Proceedings F, vol. 134, no. 2, pp. 191–197, 1987.
[13] M. Rangaswamy, D. Weiner, and A. Ozturk, "Non-gaussian random vector identification using spherically invariant random processes," Aerospace and Electronic Systems, IEEE Transactions on, vol. 29, no. 1, pp. 111–124, 1993.